Multivariate statistical analysis and Geospatial approach for evaluating Hydro-geochemical characteristics of meltwater from Shaune Garang Glacier, Himachal Pradesh, India

Ramesh Kumar[1], Rajesh Kumar[1], Anshuman Bhardwaj[2], Atar Singh[1], Shaktiman Singh[2], Anupma Kumari[3], Ravindra Kumar Sinha[3]

[1]Department of Environmental Science, School of Earth Sciences, Central University of Rajasthan, Bandar Sindri, Ajmer, India.

[2]School of Geosciences, University of Aberdeen, AB24 3UE, United Kingdom.

[3]Environmental Biology Laboratory, Department of Zoology, Patna University, Patna, India.

Abstract

The study focuses on the hydro-geochemistry of Shaune Garang glacier's meltwater concerning glacial geomorphology. Seventy-nine water samples (53 in 2016 and 26 in 2017) of ablation season were analyzed. The cations were dominant in the order $Ca^{2+} > Mg^{2+} > Na^{+} > K^{+}$, and the anions in the order $HCO_3^{-} > SO_4^{2-} > Cl^{-} > NO_3^{-}$. The result demonstrated that HCO_3^{-} were the abundant ions, accounting for 41.03 and 34.84 % of the total ionic budget (TZ). The high ionic proportions of $(Ca^{2+}+Mg^{2+})$ versus TZ^{+} and $(Ca^{2+}+Mg^{2+})$ versus $(Na^{+}+K^{+})$ were identified as the primary factors influencing dissolved ion chemistry in meltwater. Piper diagram shows that $Ca^{2+}– HCO_3^{-}$ type water is the most common, followed by $Mg^{2+}– HCO_3^{-}$. In addition, a remote sensing approach has been used to find the possible source of the chemical constituents in the meltwater. The catchment geology has been mapped on various scales, including diverse rocks and unconsolidated surface materials containing "quartz and carbonate minerals". Layered silicates (LS) and "hydroxyl-bearing minerals" are not as common as they used to be, but their availability varies greatly in the area where they are found. The distribution of Layered silicate (LS) minerals within the catchment are majorly found at lower altitudes, which implies

the weathering mechanism due to the interaction of meltwater and parental rock. Multivariate analysis revealed that CO_3 and SiO_2 weathering, sulphate dissolution, and pyrite oxidation dominate dissolved ion concentrations. Chemometric analysis of meltwater hydro-geochemistry through Principal Component Analysis (PCA) explains 72.1 % of the total variance of four PCs. PCs 1, 2, 3 and 4 explain 39.21%, 12.91%, 10.24% and 9.74% of variance respectively in 2016. Similarly, in 2017, four PCs explain 69.9.1% of the total variance. PC 1, 2, 3 and 4 can explain 26.62 %, 20.12 %, 12.64 % and 10.52 % of variance.

Keywords: Hydro-geochemistry, Geological mapping, Chemometric analysis, Shaune Garang glacier, Hydroxyl-bearing minerals.

Introduction

The Hindu Kush Himalayan Mountain ranges and the Tibetan Plateau extend across several Asian countries (Bolch et al., 2012) and are recognized as the cryospheric region beyond the polar latitudes (Bolch et al., 2019; Wood et al., 2020). The Hindu Kush Himalayas, the source of many essential river systems in Asia, are the highest mountain range (Kaser et al., 2010; Singh et al., 2020; Immerzeel et al., 2020), which provide a source of livelihood for millions of people living in this region. The Hindu Kush Himalaya, also known as the 'Third Pole' and the 'water tower of Asia,' provides ecosystem services, particularly water, the lifeblood of all organisms. The ecosystem services produced in the region provide support for 240 million people who live in the hills and mountains and approximately 1.7 billion people who live downstream in the major river basins. The increasing metropolitan infrastructure in the Himalayan region in the last three decades has put additional strain on the region's limited water resources (Tiwari et al., 2018). Other than natural forces, the primary causal variables in the Himalayas include extraordinary urbanization, increasing tourism, shifting land use patterns, garbage disposal, and agricultural runoff are all factors to consider (Thakur et al.,

2019; Kumar et al., 2019). Snow/glaciers meltwater is a vital water source for domestic use in the higher Himalayas. At the same time, it is essential for irrigation, industrial use, and hydroelectric power generation for the downstream population (Singh et al., 2008). When the other water sources are low in supply, the glacier discharge plays a more prominent role in sustaining the demand (Kumar et al., 2016; Singh et al., 2022). The meltwater drains from the glaciers meet the various soil particles and are subsequently influenced by the various mineral components. According to recent research, climate and land-use/cover changes caused by human endeavours significantly impact the chemical composition of Himalayan freshwater (Pant et al., 2021; Thapa et al., 2020). Hydrogeochemical characterization of the glacier meltwater varies between glaciers due to differential lithology (Collins, 1979). When it comes to glacier meltwater chemistry and, consequently, the quality of meltwater, the geology of the catchment is one of the most important factors to consider. Such studies also improve our understanding of the interactions of meltwater with the underlying geological strata and provide insights into the hydro-climatic regime of a region. There is a need to conduct more research in these areas to create a robust database to determine hydrochemistry confidently. The widely varying geology makes the hydro-chemical study of Himalayan glaciers even more exciting. Earlier studies on the chemistry of the major ions in the Himalayas engrossed in recognizing chemical input in glacial meltwater. Various studies of Himalayan glaciers have suggested that water transients over sub-glacial waterways encounter rock substrate experiencing a significant chemical change in meltwater (Singh et al., 2015, 2017). Some studies specify that the high degree of differential erosion in Himalayan glaciated areas is the consequence of the long interaction time of meltwater through bedrock (Haritashya et al., 2010; Singh et al., 2015). Investigating hydrochemistry in the Himalayas is highly important, and several researchers (Haritashya et al., 2010; Singh et al., 2015; Kumar et al., 2019) have contributed to this regard.

All the previous studies in the Himalayan region on water chemistry have focused only on the chemical characterization of meltwater from glaciers. Documentation of such investigations substantially allows precise lithological mapping and erosion rate estimation in these high-mountain areas. This helps in understanding large-scale links between glacio-hydrology and geochemistry. Considering possible sources and their differential erosion rates can give us a better idea about the possible future trajectory of meltwater chemistry in these high-mountain catchments. Photogrammetry, high-resolution terrain modelling and hyperspectral imaging are used in lithological mapping and estimation of erosion rates in high mountains. Further, it helps establish large-scale links between glacio-hydrology and geochemistry on a global scale.

In the present study, the remote sensing approach has been used to identify chemical species' sources of origin in meltwater through the catchment scale lithological mapping, mineral detection, and many other perspectives. Also, ASTER-SWIR data were used to delineate types of rocks in the Shaune Garang catchment to interpret and measure minerals and the geochemical composition of debris on the glacial surfaces. This study validates several features of ASTER (SWIR and TIR) data and their processing techniques; analysis has been used to map several minerals containing indices. These exploration approaches are suitable for low-cost identification and mapping of minerals containing indices such as layered silicates (LS), Calcite (CA), Hydroxyl bearing (OH), Alunite (AL) on the SWIR band and carbonate, quartz, and mafic index on TIR band in ASTER data. In this research, we focus on identifying (i) major ion concentrations, chemical characteristics, and their variability; (ii) hydro-geochemical processes and solute sources during the study period; and (iii) lithological mapping of the Shaune Garang catchment. Hence, the results of this study enrich the catchment findings in terms of glacio-hydrology and geochemistry. Furthermore, this would be a significant step towards a more precise interpretation of weathering and hydrological processes in the catchment. This research includes applying various chemometric analyses such as principal

component analysis (PCA) and factor analysis to understand better the dominant weathering process in the Shaune Garang catchment.

Study Area

The hydro-geochemical analysis has been performed in the Shaune Garang glacier catchment, located in Himachal Pradesh. The glacial meltwater of this catchment merges to the Baspa River, a stream of the Sutlej River and finally joins the Indus River system. The study area has been presented in Figure 1, where locations of the instruments like the Automatic Weather Station (AWS) discharge gauge have also been shown. The watershed and glaciated area in the catchment have also been presented along with the contour map. This catchment receives precipitation from the winter westerlies and the monsoon in summer (Singh et al. 2018), but summer precipitation dominates winter precipitation. The winter precipitation in this region is received through the Western Disturbance (WD) (Dimri 2004). This region experiences ablation from May to September (Kumar et al., 2016). It covers an area of 38.13 km^2 above the discharge site. The hypsometric distribution of the catchment is presented in Figure 2.

Hypsometry distribution clearly shows that 75% of the catchment has a non-glaciated area while 25% is glaciated. In the glaciated area, the debris-covered glacier has its share of 5%, while the debris-free glacier has 20%. The rocks of this region resemble the Higher Himalayan Crystalline. It contains pelitic and psammopelitic meta-sediments having acid and basic intrusive. Granite and gneiss rocks in the Himalayan region have a familiar presence of late-stage pegmatitic veins feldspar (Kumar et al., 1987). Rohtang gneiss is the principal constituent of the Himalayan glaciers. Chalcopyrites' presence is also noticed in lateral morainic deposits of the Himalayas. The morphology of the Shaune Garang catchment describing the area vs aspect and area vs slope has been shown in Figure 3. The aspect ratio suggests that most of the part of the catchment falls in the East and South, Southwest and West direction and receives

higher solar insolation, making it prone to weathering. Further, the primary area falls in the middle slope zone of 24° to 40° and the higher slope zone 40° to 56°, which transfers the weathered materials very quickly to the glacier.

Sampling and analysis protocol

In the higher Himalayas, the physical accessibility is limited to the summer season. Water samplings were performed during the summer seasons of 2016 and 2017 at the selected locations of the channel (Figure 1). Selected cations and anions of glacial meltwater were examined in 2016 and 2017. Fifty-three water samples in 2016 and 26 water samples in 2017 were collected during ablation season. The sampling sites were chosen as per the geology, altitude, terrain, and convergence of tributaries. Polyethylene sample bottles (250 ml) were rinsed with distilled water after being cleaned with nitric acid for accuracy in data. Water samples were taken from 20 cm deep to have a well-mixed concentration. Sampled glacial meltwater was filtered on 0.45 µm Whatman filter paper. The conductivity and pH measurements have been performed in the field by a handheld multi-parameter instrument (HANNA, model No. HI9829). The essential cations (Ca^{2+}, Mg^{2+}, K^{+} and Na^{+}) analyses were performed using Atomic Absorption Spectroscopy. The instrument has a precession of 0.05 parts per million (ppm) for Ca^{2+}, Mg^{2+}, K^{+}, Na^{+}, and 0.01 parts per million (ppm) for the remaining parameters. Ion chromatography was used to analyze the anions (Cl^{-}, SO_4^{2-} and NO_3^{-}). The bicarbonate concentration was based on the results of the titration method (APHA 2005) and the charge balance method. The precautions were made as per the specified norms, and we used non-powder vinyl cleanroom gloves and masks for sampling and analysis. A new standard of identified concentration and procedural blank was analyzed for every analytical run. During the investigation, no detectable contamination was obtained. The data from physio-chemical analysis of the meltwater samples were subjected to multivariate statistical analysis. The study used multivariate statistical tests to examine relationships among multiple variables

in the data set. Excel add-on XLSTAT was used for the analysis of normalized data under PCA. Bartlett's sphericity test was applied to both years' melting season data, and a correlation matrix was prepared. The principal component analysis has been analyzed to understand problems under different measurement scales of the original variable, which is avoided by diagonalizing the correlation matrix. The dissolved ions composition of the meltwater from Shaune Garang glacier were subjected for the error analysis in the charge balance, which has been computed through the given formula:

$$\mathrm{CBE} = \frac{(\mathrm{TZ}^{+} - \mathrm{TZ}^{-})}{(\mathrm{TZ}^{+} + \mathrm{TZ}^{-})} \times 100$$

Equation 1

Where, (TZ^+) = total cations and (TZ^-) = total anions

The errors of TZ^+ and TZ^- were < 10 % for two consecutive melting periods (2016 and 2017), which is indicative of the good quality of data.

Remote sensing data and characteristics

Air temperature of glacier surface was measured in ablation season (June to October) during the study period. Satellite data has been validated by the ground-based temperature records of snow, ice, and debris-covered glacier at twenty sites during the satellite passes at 10:30 AM over the study area. ASTER data were used in this investigation to obtain lithological and mineralogical evidence from the Shaune Garang catchment. A subset of the high-resolution and cloud-free images (ASTER) were used throughout the study to determine the precise lithological mapping of the exposed rock present in the catchment. The imagery of nine bands was used in this study, with band-1 being blue (0.43 - 0.45 µm), band-2 being blue (0.45 - 0.51µm), band-3 being green (0.53 - 0.59 µm), band-4 being red (0.64 - 0.67 µm), band-5 being

near-infrared (0.85 - 0.88 µm), band-6 being shortwave infrared (1.57 - 1.65 m), band-7: shortwave infrared (2.11 - 2.29 µm), band-8: panchromatic (0.50 - 0.68 µm), and band-9: cirus (1.36 - 1.38 µm) were used. Respective bandwidths and subsystems characteristics are presented in Table1.

Result and discussion

Hydrogeochemistry of glacial meltwater

The physical analysis of meltwater indicates a little alkaline with pH ranging from 6.86-8.56 with an average value of 7.45 ±0.48 and 7.45 ±0.45 for 2016 and 2017, respectively (Table 2). Higher pH indicates that the process of dissolution is higher due to the more considerable contact period with rock, soil and rainwater. These would have imparted alkalinity to the meltwater (Kumar et al. 2014). Electrical conductivity indirectly measures the mineralization that explains the ionic strength of water (Kumar et al., 2019). The standard value of electrical conductivity was 86.14 ±16.96 µS/cm in 2016 and 91.25 ±16.62 µS/cm in 2017. The higher EC must result from the weathering, evaporation, and crystallization processes. Furthermore, the lesser conductivity in glacier discharge is influenced by increased precipitation making higher discharge and decreased influence of the evaporite dissolution process. The measured value of EC suggests that hydrochemistry of location is regulated through the interface of water and rock and depends on the weathering of rocks. Different rocks and their solubility influence the proportional concentration of ions in glacial meltwater (Pant et al. 2021). Table 2 displays the distribution of dissolved ionic concentrations with standard deviation in the meltwater discharge of the Shaune Garang glacier.

The results presented in Table 2 indicate that Ca^{2+} contributes 39.57% and 42.53 % in the total cationic budget in both the consecutive study periods 2016 and 2017. However, Ca^{2+} + Mg^{2+} contributes 82.10 % and 71.02 % of the total cationic budget in the catchment. The other two

194 cations, Na^+ and K^+, contribute only 16.78 % and 17.57 %, respectively, during the study period
195 2016 and 2017. Bicarbonate (HCO_3^-) is the most dominant anion contributing 62.18 % and
196 54.44 %, respectively, in the total anionic budget of the ablation period of 2016 and 2017. Its
197 average concentration was observed as 369.65 ±79.41 µeq/l, and 316.73 ±83.23 µeq/l in the
198 consecutive study period. Sulphate (31.10% and 38.11 %) was the second most dominant
199 anion, followed by chloride (5.58% and 6.64 %) and Nitrate (1.18% and 0.79 %) during
200 consecutive years' observation. The dominance of bicarbonate in Shaune Garang Catchment is
201 due to the silicate dominating geomorphology of the catchment. According to the findings,
202 weathering of silicate minerals is less visible than carbonate minerals.

203 Figure 4 displays the concentration of different anions and cations and electrical conductivity
204 for the glacier's meltwater at different parts of the Indian Himalaya. The concentration of
205 cations and anions varies as per the morphology of rocks in the catchments and weather system.
206 Meltwater draining from the Himalayan region shows the dominance of Ca^{2+} and HCO_3^-,
207 whereas Bagni, Chaturangi, Gangotri and Dudu glaciers demonstrate the dominance of SO_4^{2-}
208 in their catchment. The dominating presence of silicate-bearing rocks is the important factor
209 for the higher concentration of bicarbonate (HCO_3^-) in the meltwater of the Himalayan glacier.
210 In addition, the dominancy of SO_4^{2-} in the Bagni, Chaturangi, Gangotri and Dudu glaciers could
211 be due to pyrite oxidation that enhances sulphate concentration. Cl^- and SO_4^{2-}' domination is
212 influenced by halite and sulfide oxidation and weathering of soft sulphate minerals such as
213 gypsum (Thomas et al., 2015). The chemical composition analysis reflects the dominance of
214 bicarbonate (HCO_3^-) as an anion in most of the glacial meltwater in the Himalayan region due
215 to the dissolution of atmospheric carbon dioxide and carbonate (Sharma et al., 2013; Kumar et
216 al., 2014; Singh et al., 2015). Concentration of cations in the meltwater of Dokariani, Bara
217 Shigri and Gangotri glaciers follows a trend like $Ca^{2+} > Mg^{2+} > K^+ > Na^+$ while it follows a
218 trend of $Ca^{2+} > Mg^{2+} > Na^+ > K^+$ for meltwater of Kafni and Chhota Shigri, the only alteration

in the concentration of Na^+ and K^+ for different basins. However, the Bagni glacier meltwater showed the Potassium ion as the second most abundant. In the Bara Shigri glacial, meltwater concentration of cations varied as $Ca^{2+} > Mg^{2+} > Na^+ > K^+$ like the Chhota Shigri of its vicinity and the Kafni of Kumanyu Himalaya whereas anions concentration followed the pattern of $HCO_3^- > SO_4^{2-} > NO_3^-$. It has been observed from the comparative analysis in Figure 4 that the central Indian Himalayan glacier's meltwater has the highest concentration of Ca^{2+} cation, and a similar observation is from the present study. Interestingly, the graph shows a higher concentration of anions and cations in discharge from glaciers located in the central part of the Indian Himalayan region than the glaciers in the western part.

Hydro-geochemical process in the glacial catchment

Dissolved ions in the glacial meltwater are generally contributed through rock weathering, precipitation, anthropogenic influence, and atmospheric conditions (Jeelani 2011; Kumar et al. 2019). Generally, the chemical composition of glacial meltwater is governed by the chemical weathering between the interaction of water and bedrock beneath the glacier (Kumar et al., 2009; Kumar et al., 2014; Singh et al., 2017). The cation and anion in the glacier discharge are elucidated concerning the nature of rock and its weathering processes. Dissolved solute particles present in the glacial melt are determined by the processes involved in the glacial environment. The interrelationship between the physical and chemical parameters are presented through a scatter plot (Figure 5) of (Ca^{2+}+Mg^{2+}) and (Na^++K^+) against total cation (TZ^+). A positive correlation is observed between (Ca^{2+}+Mg^{2+}) and TZ^+. It further shows a ratio ranging from 0.75 to 0.85 with an average equivalent value of 0.75 ±0.05 during the study period.

The result demonstrates that the impact of Ca^{2+}+Mg^{2+} in the glacial meltwater is comparatively high compared to the total cation TZ^+. The ratio of Ca^{2+} and Mg^{2+} determines the input source

of calcium and magnesium ions in water. $Ca^{2+}/Mg^{2+} \leq 1$ (Table 3) indicates a process of dolomite dissolution, and a value >1 recommends the dominance of silicate weathering in water (Kumar and Singh 2015). As a result, silicate weathering could be a factor in the dominant concentration of Ca^{2+} and Mg^{2+} among cations in the Shaune Garang glacial discharge. The scatter plot (Figure 5) among $Na^{+}+K^{+}$ and TZ^{+} displays a small contribution of $Na^{+}+K^{+}$ in total dissolved ion with 0.24 ±0.04 and 0.25 ±0.08 during both ablation years. The results reveal carbonate weathering as a leading factor in the glacial meltwater ionic characteristics of the Shaune Garang catchment. The large equivalent ratios 3.23 ±0.75 and 3.28 ±1.14 for $(Ca^{2+}+Mg^{2+})/(Na^{+}+K^{+})$ in the consecutive melting period of 2016 and 2017 further strengthen the understanding of carbonate weathering dominance in the catchment. High ratio of $(Ca^{2+}+Mg^{2+})/(Na^{+}+K^{+})$ and $(Ca^{2+}+Mg^{2+})/TZ^{+}$ in the glacial meltwater demonstrate that hydro-geochemistry of the meltwater of Shaune Garang catchment is mainly administrated by CO_3 weathering with a minor contribution of SiO_2. However, the evaporation process enhances the TDS concentration in water (Prasanna et al. 2010; Xing et al. 2013). The average ratio of Na^{+}/Cl^{-} was measured to be 4.77 ±2.27 and 3.83 ±1.90 in 2016 and 2017 (Table 3). The Na^{+}/Cl^{-} ratio indicates a minor contribution of atmospheric constituents in the chemical characterization of meltwater of the catchment.

The ion exchange process in the water is mainly defined because of $(Ca^{2+}+Mg^{2+})$ versus $(HCO_3^{-}+SO_4^{2-})$ (Srinivasamoorthy et al., 2008). Dominant dissolution process of calcite, dolomite, and gypsum ion exchange may shift the points rightward owing to excess of $(HCO_3^{-}+SO_4^{2-})$. Further, the reverse ion exchange process turns leftward due to a surplus $(Ca^{2+}+Mg^{2+})$. $(Ca^{2+}+Mg^{2+})$ versus $(HCO_3^{-}+SO_4^{2-})$ indicates carbonate and silicate weathering with ion exchange as leading geochemical processes in the catchment (Figure 6). The diagram displays that contribution of $(HCO_3^{-}+SO_4^{2-})$ to the total ionic concentration in the glacial meltwater is greater than the $(Ca^{2+}+Mg^{2+})$, indicating an excess of $(HCO_3^{-}+SO_4^{2-})$ which is contributed by

silicate weathering. The dominance of calcium and magnesium ions is calculated through Ca^{2+}/Na^{+} and Mg^{2+}/Na^{+} ratios, a product of weathering of CO_3 and SiO_2. The Ca^{2+}/Na^{+} ratio was observed as 2.57 ±0.80 and 2.64 ±1.06, while Mg^{2+}/Na^{+} was respectively 2.16 ±0.67 and 2.07 ±0.81 in the meltwater of Shaune Garang glacier (Table 3). This ratio shows the dominance of Ca^{2+} and Mg^{2+} over Na^{+}. The result further confirms that hydro-geochemistry is governed by weathering of CO_3 minerals in the catchment. Hydrogen ion availability is responsible for rapid CO_3 weathering (Das and Kaur 2001). Na^{+} normalizes Ca^{2+} and HCO_3^{-} concentration and determines the effect of SiO_2 weathering, evaporative dissolution or CO_3 weathering in meltwater (Kumar et al., 2015). To understand the chemical weathering, sulphate mass fraction (SMF), and the ratio of sulphate (SO_4^{2-}) to ($SO_4^{2-} + HCO_3^{-}$) have been calculated in the study catchment. The chemical characteristics of meltwater show the importance of carbonation if the SMF value is (<0.5). The SMF value indicates the chemical attributes of meltwater affected by sulfide oxidation and the termination of CO_3 (Tranter et al. 1993). In the Shaune Garang catchment, an average SMF value of 0.33 ± 0.07 and 0.41± 0.09, respectively, during the study period 2016 and 2017 indicates the dissolution of carbonate and sulfide oxidation. In Addition, C-ratio (HCO_3^{-}/ $HCO_3^{-} + SO_4^{2-}$) has also been calculated to find the significance of proton-producing effects necessary for the chemical weathering of carbonate rocks. During 2016 and 2017, the C-ratios were 0.67 ±0.07 and 0.59 ±0.09, demonstrating the domination of the carbonate and sulphate weathering processes.

Mineral mapping

The Short Wavelength Infra-Red (SWIR) and Thermal Infrared (TIR) spectral resolution agree for mapping surface mineralogy. These spectral bands are available in (ASTER) and have been used to map the distribution of minerals on supraglacial debris. Minerals are mapped through the band indices like "SWIR indices", "TIR indices", and "TIR emissivity silica weight per cent" in the Shaune Garang catchment. The mineral measurement reflects the primary presence

of quartz, feldspar, carbonate, and mica. High altitude glacier debris reflected the fact of "quartz, feldspar as calcium albite, and mica as biotite". The debris on the Shaune Garang glacier is dominated by muscovite (mica), calcium albite (feldspar) and quartz. Though in lesser quantity, the presence of calcite has also been noticed. To create thematic mineral abundance maps and quantitative estimation of minerals, "SWIR and TIR indices" have also been used (Ninomiya, 2004).

SWIR indices

Short Wavelength Infrared (SWIR) mineral indices were used to wavelength-dependent absorption patterns in estimating minerals in the catchment. The SWIR mineral indices were used to evaluate the mineral's dominance in the catchment. Equations 1, 2, 3 and 4 have been used respectively for understanding the dominance of layered silicate (LS), calcite (CA), hydroxyl-bearing (OH), and Alunite (AL).

$$\mathbf{LS} = \frac{(\mathrm{AST4} \times \mathrm{AST8})}{(\mathrm{AST5} \times \mathrm{AST6})} \quad \text{Equation 1}$$

$$\mathbf{CA} = \frac{(\mathrm{AST6} \times \mathrm{AST9})}{\mathrm{AST8}^2} \quad \text{Equation 2}$$

$$\mathbf{OH} = \frac{(\mathrm{AST4} \times \mathrm{AST7})}{\mathrm{AST6}^2} \quad \text{Equation 3}$$

$$\mathbf{AL} = \frac{\mathrm{AST7}^2}{(\mathrm{AST5} \times \mathrm{AST8})} \quad \text{Equation 4}$$

Where,

AST*n* is band number (*n)* related to ASTER

The varying indices are related to the variable absorption properties, which helps measure the types of minerals. A sensor, "radiance band ratios", can reduce the influence of the atmosphere and the topography of a region and the variation in illuminance (Abrams et al., 1983; Mather, 1987). The evidence also indicates the nonsignificant evidence in "single band or three-band true or false colour composite imageries". It is also helpful in having the quantitative estimation of mineral abundances. In this study, images of the 4-shortwave infrared (SWIR) mineral indices are displayed in Figure 7, reflecting the relative dominance of minerals and their presence on the surface. Alunite has been most dominant and abundant in higher altitudes up to the accumulation zone. "Layered silicates" and "hydroxyl-bearing minerals" are less productive, while "calcite and hydroxyl-bearing minerals" varies location-wise. Alunite index displays little white patches in the higher region with high abundance. Figure 7 shows kinematics and pulse flow movements of layered silicate debris, which can be understood through their variability and abundance. The evidence of Alunite at a higher altitude might be due to its formation mechanism. The formation of Alunite through the reaction of sulfuric acids with potassium-rich feldspars is called "alunitization". Layered silicates and "hydroxyl-bearing minerals" are in short supply, but "calcite and hydroxyl-bearing" minerals vary significantly within the catchment. Layered silicate consists of octahedral layers bound to the tetrahedral and primary component of soil. Its distribution within the catchment at lower altitudes implies the weathering mechanism due to meltwater and parental rock interaction. They have been the excellent water trapping mechanism held between layers. The essential minerals in layered silicates are kaolinite, nacrite and dickite.

TIR indices

To evaluate various minerals in the Shaune Garang catchment area, Thermal infrared (TIR) mineral indices of Carbonate, Quartz and Mafic were used. The thermal spectrum is instrumental in distinguishing the geology of earthy minerals, where TIR satellite spatial resolution is noticeably lesser than VNIR or SWIR (VNIR 15 m, SWIR 30 m, TIR 90 m). However, TIR is exclusive in targeting the profusion of carbonate, quartz, and silicate minerals. Band ratios derived from TIR estimate carbonate, quartz and silica bearing lithology (Figure 8). Equations 5, 6 and 7 were used for Carbonate Index (CI), Quartz Index (QI), and Mafic Index (MI), respectively.

$$\mathbf{CI} = \frac{\mathrm{AST13}}{\mathrm{AST14}} \qquad \text{Equation 5}$$

$$\mathbf{QI} = \frac{\mathrm{AST11}^2}{(\mathrm{AST10} \times \mathrm{AST12})} \qquad \text{Equation 6}$$

$$\mathbf{MI} = \frac{(\mathrm{AST12} \times \mathrm{AST14}^3)}{(\mathrm{AST133})} \qquad \text{Equation 7}$$

Where,

"ASTn is band number (n) based on the properties of ASTER spectral

The CI is better used to detect primary carbonate minerals such as "calcite and dolomite". These two carbonates mineral have higher absorption features, which indicates the availability of calcite and dolomite. The absorption features of calcite are about 11.4 to 11.2 μm in the case of dolomite minerals. Minerals of carbonates with "hydrothermal origin" are very challenging

to identify through a CI map due to an inadequate percentage of carbonate presence. However, calcite-bearing propylitic alteration is accredited as the "ASTER TIR" feature. The chlorite and epidote had lower emissivity between TIR bands 11 and 13 but slightly higher between 13 and 14 (Salisbury et al. 1992). Aspects of the spectrum with these characteristics resemble the mafic index minerals. Mafic and quartz index minerals found uneven distribution within the catchment, but carbonate minerals were found at lower altitudes along the riverside. The reason behind the occurrence of carbonate minerals along river channels might be due to the higher weathering across the river.

Chemometric Analysis

Principal component and factor analysis

Excel add-on XLSTAT was used for the analysis of normalized data under PCA. The sphericity test of Bartlett was performed on the data of both years. The Bartlett sphericity test shows that observed $\chi 2$ (342.85) is considerably more significant than the critical $\chi 2$ (85.96) in 2016 and $\chi 2$ (observed) = 125.25 larger than the critical value $\chi 2$ (critical) = 48.3 in 2017. The principal component analysis helped to understand problems under different measurement scales of the original variable avoided by diagonalizing the correlation matrix.

Table 4 demonstrates the PC value of more than 1, which explains 72.1 % of the total variance of four PCs. PCs 1, 2, 3 and 4 are capable of explaining 39.21%, 12.91%, 10.24% and 9.74% of variance in 2016. Similarly, in 2017 scree plot (Figure 9) shows four PCs, which explains 69.9.1% of the total variance. PC 1, 2, 3 and 4 can explain 26.62 %, 20.12 %, 12.64% and 10.52 % of variance. Table 4 further depicts the Eigenvalues, the percentage of variance calculated through varimax rotation matrix with Kaiser Normalization and rotated factor, and the percentage of variance in each PC. High SO_4^{2-} and K^+ loadings are observed in both the years, indicating silicate weathering dominance in the catchment. Moderately high loading

384 values of Ca^{2+}, Mg^{2+} and Na^{+} in both years indicate the dominance of the process, which is
385 prevailing in factor 1.

386 Table 5 indicates that factor 4 shows the negative pH in both the years and the acceptable value
387 of Cl^{-} in the consecutive study period. The first two principal component loading are presented
388 to understand the grouping and relationship of all chemical parameters. The PC loading has
389 been calculated to understand correlations among variables and know the most influential
390 variables. It could result from the minerals present in the soil (Yakubo et al., 2009). Throughout
391 the study, higher loadings in Na^{+} and Mg^{2+} may be accredited to the ionic conversation between
392 water through dissolution minerals containing sodium.

393 Statistically, the coefficient of determination (R^2) indicates one variable's level of statistical
394 agreement with another. Here, it is applied among the hydrogeochemical parameters and
395 represented in (Table 6) during the study period. Water chemistry parameters such as EC and
396 Na^{+} are highly interrelated with Ca^{2+}, Mg^{2+}, and HCO_3^{-}. Similarly, a decent relationship among
397 (Ca^{2+}- Mg^{2+}), (Ca^{2+} - HCO_3^{-}) and (Mg^{2+} - HCO_3^{-}) has been observed. The above parameters
398 have a good positive correlation ($R^2 > 0.5$) and are an indicator of control by these parameters
399 in the solute chemistry of the study region. The strong correlation between parameters such as
400 Ca^{2+}, Mg^{2+}, (Ca^{2+} - HCO_3^{-}), (Mg^{2+} - HCO_3^{-}) indicates strong carbonate weathering (Singh et
401 al., 2017). In the case of sulphate (SO_4^{2-}) ion concentration, it shows a good relationship with
402 Ca^{2+} and Mg^{2+}, indicating the sulphate mineral's high dissolution in the glacier's catchment.

403 **Hydro-geochemical facies of the glacial meltwater**

404 Hydrogeochemical facies of the meltwater helps interpret the dominant anions and cations,
405 which have been determined through a Piper plot (Figure 10). It is used to find similarities and
406 dissimilarities among all water types, where the analogous water qualities fall together (Todd,
407 2001). In the cation plot, it can be seen that most of the water is concentrated in a trilinear

pattern in the middle, indicating that it is a mixed water type. The calcium ions predominate in the glacial discharge. The hydro-geochemical cations in the bottom left triangle of Shaune Garang glacial discharge prove calcium ions' dominance. It substantiates the conclusions reached in the sections on hydro-geochemistry and hydro-geochemical processes, both included in the previous section. Slightly elevated sodium and potassium ion concentrations in several samples confirm the presence of sources at the various sampling locations of the Shaune Garang catchment. This must be contributing to the overall cation concentration (Karim and Veizer, 2000; Ravikumar, 2017). The Piper plot aids in the understanding of the fact, Ca^{2+}, Mg^{2+} and HCO_3^- are the most prevalent ions in the Shaune Garang catchment. The average percentage value of (Ca^{2+}+ Mg^{2+}) is about 77% and 81%, respectively in the years 2016 and 2017; however, for the (Na^++ K^+) it showed about 33 % and 29%, respectively, demonstrating that alkaline earth metals are prevailing over alkali metals (Singh et al., 2017). It further supports the dominance of dolomitic limestone containing gypsum and pyrite in the region (Figures 7 and 8). The piper diagram demonstrates that carbonate type weathering has been more instrumental in governing hydro-geochemistry in this catchment. The figure indicates the presence of the (Ca^{2+}– HCO_3^-) type of water with little influence from (Ca^{2+}– SO_4^{2-}) type. Significant ions and TDS were found in higher concentrations in this catchment, indicating more significant interactive processes between rock materials and water having influential weathering due to moisture.

Apart from the Piper plot, Gibb's diagram (Gibbs 1970) was applied to understand how hydro-geochemical techniques such as precipitation, rock-water interface, and vaporization impact the environment's hydrogeology. According to the Gibbs diagram (Figure 11), the chemical weathering of rock minerals and a minimal extent of evaporation crystallisation are the essential variables to consider the meltwater quality in the Shaune Garang catchment. Gibb's diagram advocates the higher rock-water interaction resulting in higher ionic concentration in

meltwater. Chemical weathering, carbonate dissolution and ionic exchange between water and clay indicate the rock-water interaction processes (Kumar et al., 2014). Increased evaporation, chemical weathering and anthropogenetic actions raise the total dissolved solids. Furthermore, the findings show that water contamination from poor sanitation has increased Na^+ and Cl^- ions and increased total dissolved solids (TDS) (Kumar et al., 2014).

Conclusion

The current study focused on the hydro-chemical analysis of meltwater from the Shaune Garang catchment, located within the Baspa Basin. According to the findings, meltwater is slightly alkaline with Ca^{2+} and HCO_3^- the most prevalent ions during the study. Ca^{2+} and Mg^{2+} were the dominant cations constituting (41.03%, 42.53%) and (34.84%, 32.89%) of the total cationic budget in the consecutive study period. The predominance of carbonate weathering is indicated by the ratio of $(Ca^{2+}+Mg^{2+})/(Na^++K^+)$ and $(Ca^{2+}+Mg^{2+})/(TZ^+)$ and a strong positive association between Ca^{2+}– Mg^{2+}, Ca^{2+}– HCO_3^- and Mg^{2+}– HCO_3^-. Piper plot demonstrated that alkaline earth metal dominates alkali metal, and weak acid exceeds strong acid. This plot also indicated that the Ca^{2+}– HCO_3^- is most influential, assessed by Mg^{2+}–HCO_3^- type of water in this area. The Gibbs plot also revealed that rock corrosion is the primary process regulating meltwater concentration. The values in the chloro-alkaline indices in this study were negative, indicating the conversation of Ca^{2+} and Mg^{2+} ions by Na^+ and K^+ ions of rock material. The geological mapping of the catchment has been done on varying scales, including diversified rocks and unconsolidated surface materials that possess "quartz and carbonate minerals". The results were verified through the geological, stratigraphic, and structural maps in the multifaceted lithological terrain of the region. Based on the lithological map of the Shaune Garang catchment, Layered silicates and "hydroxyl-bearing minerals" are less abundant. However, "calcite and hydroxyl-bearing minerals" have significantly varying availability in the catchment. The distribution of Layered silicate minerals within the catchment is majorly found

458 at lower altitudes, which implies the weathering mechanism due to the interaction of meltwater
459 and parental rock. The chemometric analysis includes a principal component (PC),
460 eigenvalues, the percentage of variance calculated through varimax rotation matrix with Kaiser
461 Normalization and rotated factor, and the percentage of variance in each PC. High SO_4^{2-} and
462 K^+ loadings are observed in both years, indicating silicate weathering dominance in the
463 catchment. Moderately high loading values of Ca^{2+}, Mg^{2+} and Na^+ in both years indicate the
464 dominance of the process, which is prevailing in factor 1. The strong correlation between
465 parameters such as Ca^{2+}, Mg^{2+}, (Ca^{2+} - HCO_3^-), (Mg^{2+} - HCO_3^-) indicates intense carbonate
466 weathering (Singh et al. 2017). In the case of sulphate (SO_4^{2-}) ion concentration, it shows a
467 good relationship with Ca^{2+} and Mg^{2+}, indicating the sulphate mineral's high dissolution in the
468 glacier's catchment.

469 **Acknowledgement**

470 The present support of the Department of Science and Technology as a research project
471 (DST/CCP/NHC/159/2018(G)) became instrumental in utilising the human resources for the
472 analysis of the results. The financial support of the USAID project (CHARIS) for carrying out
473 fieldwork is thankfully acknowledged. The analysis is made at the DST supported FIST Lab
474 in the Department of Environmental Science, Central University of Rajasthan. The support is
475 thankfully acknowledged.

476 **Declaration of interests**

477 The authors declare no competing financial or personal interests that influenced their work.

478 **References:**

479 Abrams, M.J., Brown, D., Lepley, L., Sadowski, R (1983) Remote sensing for porphyry
480 copper deposits in southern Arizona. Economic Geology. 78(4), 591–604.
481 https://doi.org/10.2113/gsecongeo.78.4.591.

APHA (2005). Standard methods for the examination of water and wastewater (p. 1220). American Public Health Association.

Bishwakarma, K., Pant, R. R., Pal, K. B., Ghimire, A., Thapa, L. B., Saud, P., Joshi, S., & Panthi, K. P (2019). Water quality and land use/cover changes in the Phewa Watershed, Gandaki Province, Nepal. Nepal Journal of Environmental Science, 7, 31–39. https://doi.org/10.3126/njes.v7i0.34473.

Bolch, T., Kulkarni, A.V., Kääb, A., Huggel, C., Paul, F., Cogley, J.G., Frey, H., Kargel, J.S., Fujita, K., Scheel, M., Bajracharya, S., Stoffel, M (2012) The state and fate of Himalayan glaciers. Science, 336(6079), 310–314. DOI: 10.1126/science.1215828.

Brown, G.H., Sharp, M.J., Tranter, M., Gurnell, A.M., Nienow, P.W (1994) The impact of post-mixing chemical reactions on the major ion chemistry of bulk meltwaters draining the Haut Glacier d'Arolla, Valais, Switzerland. Hydrological Process. 8:465–480. https://doi.org/10.1002/hyp.3360080509.

Chidambaram, S., Karmegam, U., Prasanna, M.V., Sasidhar. P., Vasanthavigar, M (2011) A study on the hydro-chemical elucidation of coastal groundwater in and around Kalpakkam region, Southern India. Environmental Earth Science. 64(5), 1419–1431. https://doi.org/10.1007/s12665-011-0966-3.

Das, B.K., Kaur, P (2001) Major ion chemistry of Renuka Lake and weathering processes, Simaur District, Himachal Pradesh, India. Environmental Geology. 40:908–917. https://doi.org/10.1007/s002540100268.

Dimri, A.P (2004) Impact of horizontal model resolution and orography on the simulation of a western disturbance and its associated precipitation. Meteorological Application. 11, 115–127. DOI:10.1017/S1350482704001227.

Dutta, S., Mujtaba, S.A.I., Saini, H.S., Chunchekar, R., Kumar, P (2017) Geomorphic evolution of glacier-fed Baspa Valley, NW Himalaya: record of Late Quaternary climate change, monsoon dynamics and glacial fluctuations. In: Pant NC, Ravindra R, Srivastava D, Thompson LG (eds) The Himalayan cryosphere: past and present, Special Publications, 462. Geological Society, London. https://doi.org/10.1144/SP462.5.

Fu, B., Chou, X (1998) Thermal infrared spectra and TIMS imagery features of sedimentary rocks in the Kalpin Uplift, Tarim Basin, China. Geocarto International. 13, 69–73. https://doi.org/10.1080/10106049809354630.

Gabr, S., Ghulam, A., Kusky, T (2010) Detecting areas of high-potential gold mineralisation using ASTER data. Ore Geology Reviews. 38, 59-69. https://doi.org/10.1016/j.oregeorev.2010.05.007.

Gabr, S.S., Hassan, S.M., Sadek, M.F (2015) Prospecting for new gold-bearing alteration zones at El-Hoteib area, South Eastern Desert, Egypt, using remote sensing data analysis. Ore Geology Reviews. 71, 1–13. https://doi.org/10.1016/j.oregeorev.2015.04.021.

Gad, S., Kusky, T (2007) ASTER spectral ratioing for lithological mapping in the Arabian–Nubian shield, the Neoproterozoic Wadi Kid area, Sinai, Egypt. Gondwana Research. 11(3), 326-335. https://doi.org/10.1016/j.gr.2006.02.010.

Galy A, France-Lanord C (1999) Weathering processes in the GangesBrahmaputra basin and the riverine alkalinity budget. Chem Geol 159:31–60. https://doi.org/10.1016/S0009-2541(99)00033-9.

Gibbs, R. J (1970). Mechanisms controlling world water chemistry. Science, 170, 1088–1090. https://doi.org/10.1126/science.170.3962.1088.

Han, H., Liu, S., Wang, J., Wang, Q., Xie, C (2010) Glacial runoff characteristics of the Koxkar Glacier, Tuomuer-Khan Tengri Mountain Ranges, China. Environmental Earth Science. 61:665–674. https://doi.org/10.1007/s12665-009-0378-9.

Haritashya, U.K., Kumar, A., Singh, P (2010) Particle size characteristics of suspended sediment transported in meltwater from the Gangotri Glacier, central Himalaya — An indicator of subglacial sediment evacuation. Geomorphology. 122(1-2), 140-152. https://doi.org/10.1016/j.geomorph.2010.06.006.

Jeelani, G.H., Bhat, N.A., Shivanna, K., Bhat, M.Y (2011) Geochemical characterisation of surface water and spring water in SE Kashmir Valley, western Himalaya: implications to water–rock interaction. Journal of Earth System Science. 120 (5), 921–932. https://www.ias.ac.in/article/fulltext/jess/120/05/0921-0932.

Karim A, Veizer J (2000) Weathering processes in the Indus River Basin: implications from riverine carbon, sulfur, oxygen, and strontium isotopes. Chem Geol 170:153–177.

Kaser, G., Grobhauser, M., Marzeion, B (2010) Contribution potential of glaciers to water availability in different climate regimes. Proceedings of the National Academy of Science, USA. 107 (47), 20223–20227. https://doi.org/10.1073/pnas.1008162107.

Khadka UR, Ramanathan AL (2012) Major ion composition and seasonal variation in the Lesser Himalayan lake: case of Begnas Lake of the Pokhara Valley, Nepal. Arab J Geosci 6:4191–4206. https ://doi.org/10.1007/s12517-012-0677-4.

Kumar R, Kumar R, Singh A, Singh S, Bhardwaj A, Kumari A, Sinha RK, Gupta A (2019) Hydro-geochemical analysis of meltwater draining from Bilare Banga glacier, Western Himalaya. Acta Geophysica 67:651. https://doi.org/10.1007/s11600-019-00262-w.

Kumar R, Kumar R, Singh A, Sinha RK, Kumari A (2018) Nanoparticles in glacial meltwater. Mater Today Proc 5(3P1):9161–9166. https://doi.org/10.1016/j.matpr.2017.10.037.

Kumar R, Kumar R, Singh A, Sinha RK, Kumari A, Gupta A, Singh J (2019) Distribution of trace metal in Shaune Garang catchment: evidence from particles and nanoparticles. Mater Today Proc 15(3):586–594. https://doi.org/10.1016/j.matpr.2019.04.125.

Kumar R, Kumar R, Singh S, Singh A, Bhardwaj A, Kumari A, Randhawa SS, Saha A (2018) Dynamics of suspended sediment load with respect to summer discharge and temperatures in Shaune Garang glacierised catchment, Western Himalaya. Acta Geophysica. https://doi.org/10.1007/s11600-018-0184-4.

Kumar R, Singh S, Kumar R, Singh A, Bhardwaj A, Sam L, Randhawa SS, Gupta A (2016) Development of a Glacio hydrological model for discharge and mass balance reconstruction. J Water Resource Management. https://doi.org/10.1007/s11269-016-1364-0.

Kumar, A., Singh, C.K (2015) Characterisation of Hydro geochemical Processes and Fluoride Enrichment in Groundwater of South-Western Punjab. Water Quality, Exposure and Health, 7(3), 373-387. https://doi.org/10.1007/s12403-015-0157-7.

Kumar, A., Verma, A., Dobhal, D.P., Mehta, M., Kesarwani, K (2014) Climatic control on extreme sediment transfer from Dokriani Glacier during monsoon, Garhwal Himalaya (India). Journal of Earth System Science. 123, 109–120. https://doi.org/10.1007/s12040-013-0375-y.

569 Kumar, K., Miral, M.S., Joshi, S., Pant, N., Joshi, V., Joshi L.M (2009) Solute dynamics of
570 meltwater of Gangotri glacier, Garhwal Himalaya, India. Environmental Geology. 58,
571 1151–1159. https://doi.org/10.1007/s00254-008-1592-6.

572 Kumar, R., Kumar, R., Singh, S., Singh, A., Bhardwaj, A., Chaudhary, H (2019)
573 Hydro-geochemical characteristics of glacial meltwater from Naradu Glacier catchment,
574 Western Himalaya. Environmental Earth Sciences (2019) 78:683.
575 https://doi.org/10.1007/s12665-019-8687-0.

576 Kumar, S., Rai, H., Purohit K.K., Rawat, B.R.S. and Mundepi, A.K (1987) Chhota Shigri
577 glacier. New Delhi: Department of Science and Technology, Technical Report 1, 1–29.

578 Mather, P.M (1987) Computer Processing of Remotely Sensed Images. An Introduction, 1st
579 Edition, Wiley, Chichester.

580 Mortatti J, Probst JL (2003) Silicate rock weathering and atmospheric/soil CO2 uptake in
581 the Amazon basin estimated from river water geochemistry: seasonal and spatial variations.
582 Chem Geol 197:177–196. http://dx.doi.org/10.1016/S0009-2541(02)00349-2.

583 Ninomiya, Y (2004) Lithologic mapping with multispectral ASTER TIR and SWIR data.
584 Proceeding, SPIE, 5234, 180–190. https://doi.org/10.1117/12.511902.

585 Pant, R. R., Bishwakarma, K., Basnet, B. B., Pal, K. B., Karki, L., Dhital, Y. P., Bhatta, Y.
586 R., Pant, B. R., & Thapa, L. B (2021). Distribution and risk appraisal of dissolved trace
587 elements in Begnas Lake and Rupa Lake, Gandaki Province, Nepal. SN Applied Science, 3,
588 1–13. https://doi.org/10.1007/s42452-021-04516-5.

589 Pant, R.R., Qaiser, F.U.R., Wang, G., Adhikari, S., Bishwakarma, K., Baral, U., Rimal, B.,
590 Bhatta, Y. R., Rijal, K (2021) Hydrochemical appraisal and solute acquisitions in Seti River
591 Basin, Central Himalaya, Nepal. Environ Monit Assess 193, 656.
592 https://doi.org/10.1007/s10661-021-09437-9.

593 Piper AM (1944) A graphic procedure in the geochemical interpretation of water analyses.
594 EOS Trans Am Geophys Union 25(6):914–928. https://doi.org/10.1029/TR025i006p00914.

595 Prasanna, M.V., Chidambaram, S., Srinivasamoorthy, K (2010) Statistical analysis of the
596 hydro geochemical evolution of groundwater in hard and sedimentary aquifers system of
597 Gadilam river basin, South India. Journal of King Saud University – Science. 22:133–145.
598 https://doi.org/10.1016/j.jksus.2010.04.001.

Quinton, W.L., Pomeroy, J.W (2006) Transformations of runoff chemistry in the Arctic tundra, Northwest Territories, Canada. Hydrological Process, 20, 2901–2919. https://doi.org/10.1002/hyp.6083.

Ravikumar P (2017) Somashekar RK (2017) Principal component analysis and hydro-chemical facies characterisation to evaluate groundwater quality in Varahi river basin, Karnataka state, India. Appl Water Sci 7:745–755. https://doi.org/10.1007/s13201-015-0287-x.

Rowan, L.C., Mars, J. C (2003) Lithologic mapping in the Mountain Pass, California area using advanced spaceborne thermal emission and reflection radiometer (ASTER) data. Remote Sensing of Environment, 84(3): 350-366. https://doi.org/10.1016/S0034-4257(02)00127-X.

Sabins, F.F (1999) Remote sensing for mineral exploration. Ore Geology Reviews. 14(3), 157-183. https://doi.org/10.1016/S0169-1368(99)00007-4.

Sadashivaiah C, Ramakrishnaiah CR (2008) Ranganna G (2008) Hydrochemical Analysis and Evaluation of Groundwater Quality in Tumkur Taluk, Karnataka State, India. Int J Environ Res Public Health 5(3):158–164. https://doi.org/10.3390/ijerph5030158.

Salisbury, J.W., D'Aria, D.M (1992) Emissivity of terrestrial materials in the 8–14 μm atmospheric window. Remote Sensing of Environment. 42(2), 83-106. https://doi.org/10.1016/0034-4257(92)90092-X.

Sharma P, Ramanathan AL, Pottakkal J (2013) Study of solute sources and evolution of hydrogeochemical processes of the Chhota Shigri Glacier meltwaters, Himachal Himalaya, India. Hydrol Sci J 58(5):1128–1143. https://doi.org/10.1080/02626667.2013.802092.

Sharma, P., Ramanathan, A.L., Pottakkal, J.G (2013) Study of solute sources and evolution of hydrogeochemical processes of the Chhota Shigri glacier meltwaters, Himachal Pradesh, India. Hydrological Science Journal. 58(5), 1128–1143. https://doi.org/10.1080/02626667.2013.802092.

Singh S, Kumar R, Bhardwaj A, Kumar R, Singh A (2018) Changing climate and glacio-hydrology: a case study of Shaune Garang basin, Himachal Pradesh. Int J Hydrol Sci Technol. https://doi.org/10.1504/IJHST.2018.10010353.

628 Singh S, Kumar R, Bhardwaj A, Sam L, Shekhar M, Singh A, Kumar R, Gupta A (2016c)
629 Changing climate and glacio-hydrology in Indian Himalayan Region: a review. Wiley
630 Interdiscip Rev Clim Chang 7(3):393–410. https://doi.org/10.1002/wcc.39.

631 Singh, C.K., Kumar, A., Shashtri, S., Kumar, A., Kumar, P., Mallick, J (2017) Multivariate
632 statistical analysis and geochemical modeling for geochemical assessment of groundwater
633 of Delhi, India", Journal of Geochemical Exploration. 175, 59-71.
634 https://doi.org/10.1016/j.gexplo.2017.01.001.

635 Singh, P., Haritashya, U.K., Kumar, N (2008) Modelling and estimation of different
636 components of streamflow for Gangotri Glacier basin, Himalayas. Hydrological Sciences
637 Journal. 53(2):309–322. https://doi.org/10.1623/hysj.53.2.309.

638 Singh, V.B., Ramanathan, A.L (2017) Hydro-geochemistry of the Chhota Shigri glacier
639 meltwater, Chandra basin, Himachal Pradesh, India: solute acquisition processes, dissolved
640 load, and chemical weathering rates. Environmental Earth Science, 76:223.
641 https://doi.org/10.1007/s12665-017-6465-4.

642 Singh, V.B., Ramanathan, A.L., Kuriakose, T (2015) Hydrogeochemical assessment of
643 meltwater quality using major ion chemistry: a case study of Bara Shigri glacier, Western
644 Himalaya, India. National Academy of Science Letter. 38(2), 147–151.
645 https://doi.org/10.1007/s40009-014-0310-z.

646 Srinivasamoorthy, K., Chidambaram, S., Prasanna, M.V (2008) Identification of major
647 sources controlling Groundwater Chemistry from a hard rock terrain- A case study from
648 Mettur taluk, Salem district, Tamilnadu, India. Journal of Earth System Sciences. 117(1),
649 49–58. https://doi.org/10.1007/s12040-008-0012-3.

650 Tangestani, M.H., Jaffari, L., Vincent, R.K., Sridhar, B.M (2011) Spectral characterisation
651 and ASTER-based lithological mapping of an ophiolite complex: A case study from Neyriz
652 ophiolite, SW Iran. Remote Sensing of Environment, 115(9): 2243-2254.
653 https://doi.org/10.1016/j.rse.2011.04.023.

654 Thakur, N., Rishi, M., Keesari, T., Sharma, D. A. & Sinha, U. K (2019). Assessment of
655 recharge source to springs in upper Beas basin of Kullu region, Himachal Pradesh, India
656 using isotopic signatures. Journal of Radioanalytical and NuclearChemistry1–9.
657 https://doi.org/10.1007/s10967-019-06617-3.

658 Thapa, B., Pant, R. R., Thakuri, S., & Pond, G (2020). Assessment of spring water quality
659 in Jhimruk River Watershed, Lesser Himalaya, Nepal. Environment of Earth Science, 79,
660 1–14. https://doi.org/10.1007/s12665-020-09252-4.

661 Thomas J, Joseph S, Thrivikramji KP (2015) Hydrochemical variations of a tropical
662 mountain river system in a rain shadow region of the southern Western Ghats, Kerala, India.
663 Appl Geochem 63:456–471. https://doi.org/10.1016/j.apgeochem.2015.03.018.

664 Tiwari, P. C., Tiwari, A. & Joshi, B (2018). Urban growth in Himalaya: understanding the
665 process and options for sustainable development. Journal of Urban and Regional Studies on
666 Contemporary India 4(2), 15–27. http://doi.org/10.15027/45582.

667 Todd, D.K (2001) Groundwater hydrology. Wiley, Hoboken.

668 Tranter, M., Brown, G., Raiswell, R., Sharp, M. and Gurnell, A (1993) A Conceptual Model
669 of Solute Acquisition by Alpine Glacier Meltwaters. Journal of Glaciology, 39, 573-581.
670 https://doi.org/10.3189/S0022143000016464.

671 Van der Meer, F.D., Van der Werff, H.M., van Ruitenbeek, F.J., Hecker, C.A., Bakker,
672 W.H., Noomen, M.F., Woldai, T (2012) Multi-and hyperspectral geologic remote sensing:
673 A review. International Journal of Applied Earth Observation and Geoinformation. 14(1):
674 112-128. https://doi.org/10.1016/j.jag.2011.08.002.

675 Wulf, H., Bookhagen, B., Scherler, D (2010) Seasonal precipitation gradients and their
676 impact on fluvial sediment flux in the Northwest Himalaya. Geomorphology. 118, 13–21.
677 https://doi.org/10.1016/j.geomorph.2009.12.003.

678 Xing, L., Guom, H., Zhan, Y (2013) Groundwater hydro-chemical characteristics and
679 processes along flow paths in the North China Plain. Journal of Asian Earth Science. 70–
680 71:250–264. https://doi.org/10.1016/j.jseaes.2013.03.017.

681 Yakubo, B.B., Yidana, S.M., Nti, E (2009) Hydrochemical analysis of groundwater using
682 multivariate statistical methods—the Volta region, Ghana. KSCE Journal of Civil
683 Engineering. 13(1), 55–63. https://doi.org/10.1007/s12205-009-0055-2.

684 Bolch, T., Shea, J. M., Liu, S., Azam, F. M., Gao, Y., Gruber, S., et al. (2019) Status and
685 Change of the Cryosphere in the Extended Hindu Kush Himalaya Region. In: Wester, P.,
686 Mishra, A., Mukherji, A., Shrestha, A. (eds) The Hindu Kush Himalaya Assessment.
687 Springer, Cham. https://doi.org/10.1007/978-3-319-92288-1_7.

Wood LR, Neumann K, Nicholson KN, Bird BW, Dowling CB and Sharma S (2020) Melting Himalayan Glaciers Threaten Domestic Water Resources in the Mount Everest Region, Nepal. Front. Earth Sci. 8:128. doi: 10.3389/feart.2020.00128.

Singh, R., Kumar, R., Bahuguna, I.M., Kumar, R. (2020) Grain Size Analysis of Dune and Bar Sediments of the Shyok River between Khalsar and Hunder Village, Karakoram Range, Ladakh, India. J Geol Soc India 95, 183–189. https://doi.org/10.1007/s12594-020-1408-1.

Singh, R., Kumar, R., Latief, S.U., Kumar, R., Shekhar, M. (2022). Recession of Gaglu Glacier, Chandra Basin, Western Indian Himalaya. In: Rani, S., Kumar, R. (eds) Climate Change. Springer Climate. Springer, Cham. https://doi.org/10.1007/978-3-030-92782-0_5.

Immerzeel, W.W., Lutz, A.F., Andrade, M., Bahl, A., Biemans, H., Bolch, T., Hyde, S., Brumby, S., Davies, B.J., Elmore, A.C., Emmer, A., Feng, M., Fernández, A., Haritashya, U., Kargel, J.S., Koppes, M., Kraaijenbrink, P. D. A., Kulkarni, A. V., Mayewski, P. A., Nepal, S., Pacheco, P., Painter, T. H., Pellicciotti, F., Rajaram, H., Rupper, S., Sinisalo, A., Shrestha, A. B., Viviroli, D., Wada, Y., Xiao, C., Yao, T., Baillie, J. E. M (2020). Importance and vulnerability of the world's water towers. Nature 2020, 577, 364–369.

List of figures

Figure 1: Shaune Garang glacier showing the glacial boundary, river, and water sampling sites. Sampling locations are numbered in ascending order from higher altitudes to lower altitudes.

Figure 2: Hypsometry of the Shaune Garang catchment derived from the Landsat 8 image (Kumar et al., 2016)

Figure 3: The basin's area (%) vs aspect and slope distribution (Kumar et al., 2018).

Figure 4: The average hydro-geochemical characteristics of glacial meltwater from Shaune Garang Glacier and its comparison with the other Himalayan glaciers.

Figure 5: Scatter plot of (Ca^{2+}+Mg^{2+}) against TZ^{+} and (Na^{+}+K^{+}) against total cation (TZ^{+}) during the study period of 2016 and 2017 from Shaune Garang glacier catchment.

Figure 6: Scatter plot of (Ca^{2+}+Mg^{2+}) against (HCO_3^{-}+SO_4^{2-}) and (Ca^{2+}+Mg^{2+}) against SO_4^{2-} during the study period of 2016 and 2017 from Shaune Garang glacier catchment.

Figure 7: Mineralogical maps based on the radiance properties of ASTER SWIR of Shaune Garang catchment. The indexes are represented through LS, CA, AL, and OH for layered silicate, calcite, Alunite, and hydroxyl bearing materials.

Figure 8: Mineralogy maps based on the "ASTER TIR" of Shaune Garang catchment's radiance properties. The indexes are "Carbonate Index (CI), Quartz Index (QI), and Mafic Index (MI)".

Figure 9: Scree plot graph between eigenvalue and factors for 2016 and 2017.

Figure 10: Piper plot for concentration of ions during study period 2016 and 2017 in the Shaune Garang catchment.

Figure 11: Gibb's diagram represents controlling factors of meltwater quality.

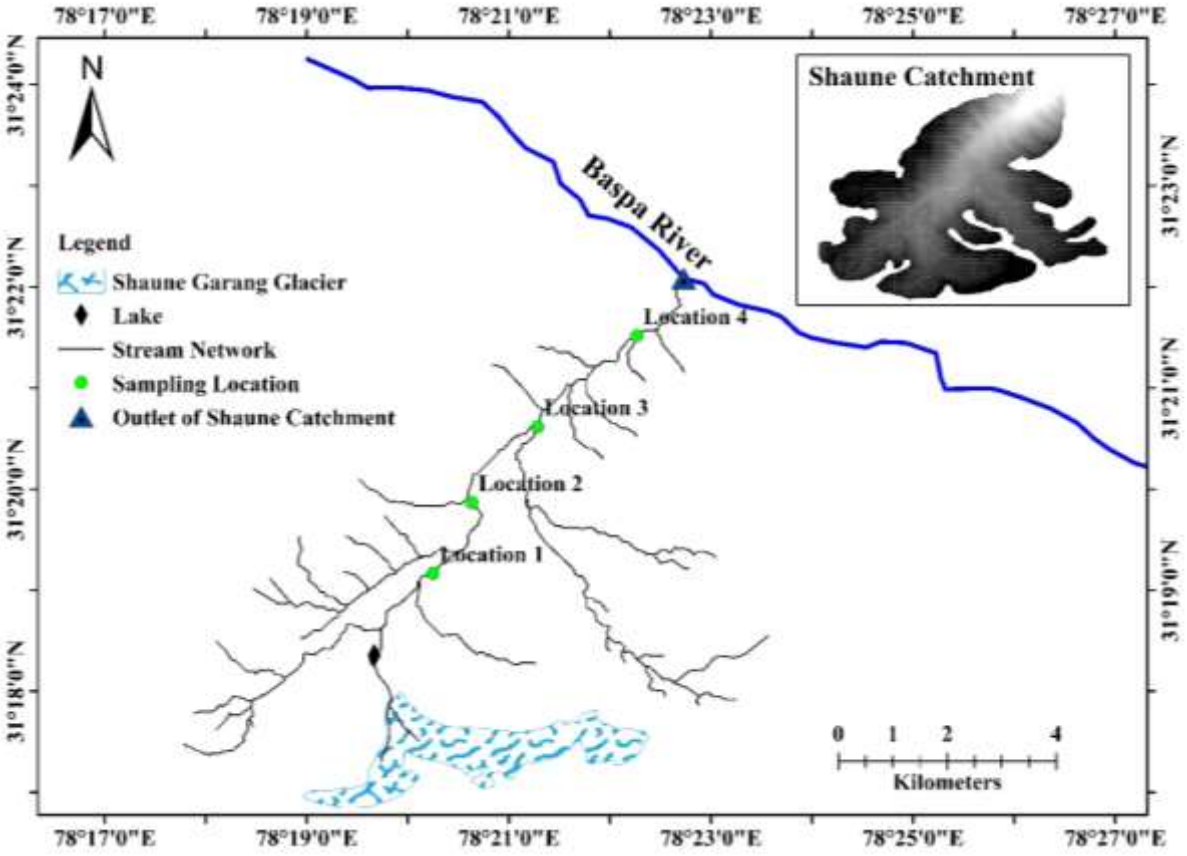

744 **Figure 1:** Shaune Garang glacier showing the glacial boundary, river, and water sampling sites.

745 Sampling locations are numbered in ascending order from higher altitudes to lower altitudes.

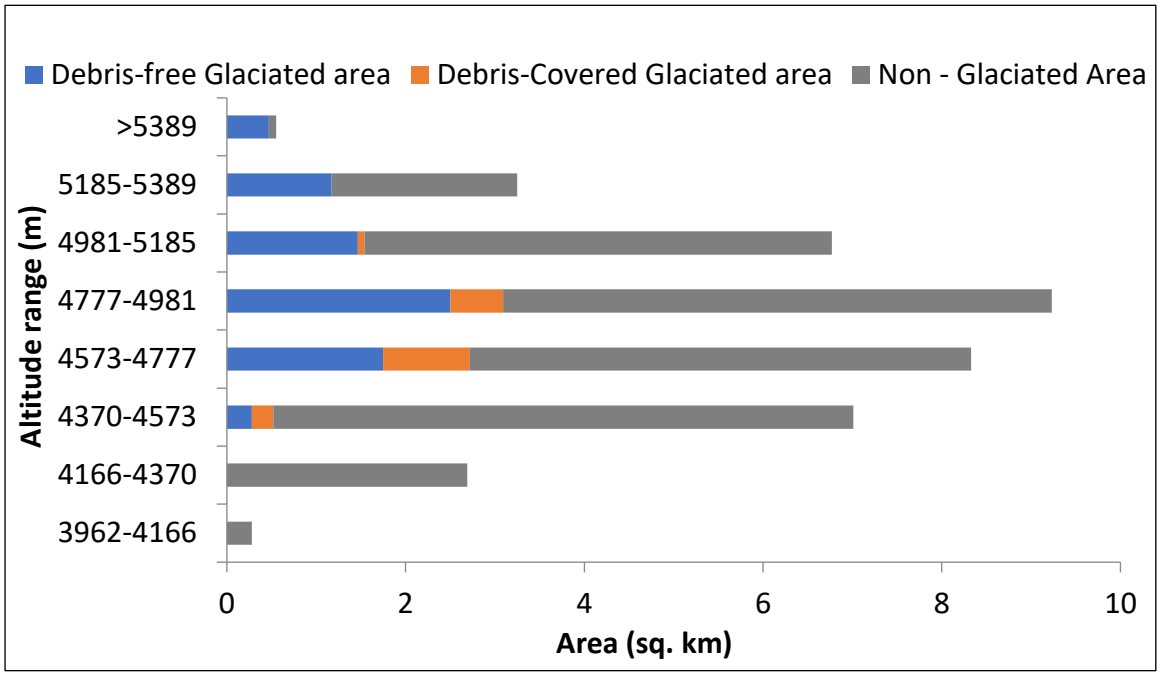

746

747 **Figure 2:** Hypsometry of the Shaune Garang catchment derived from the Landsat 8 image
748 (Kumar et al., 2016).

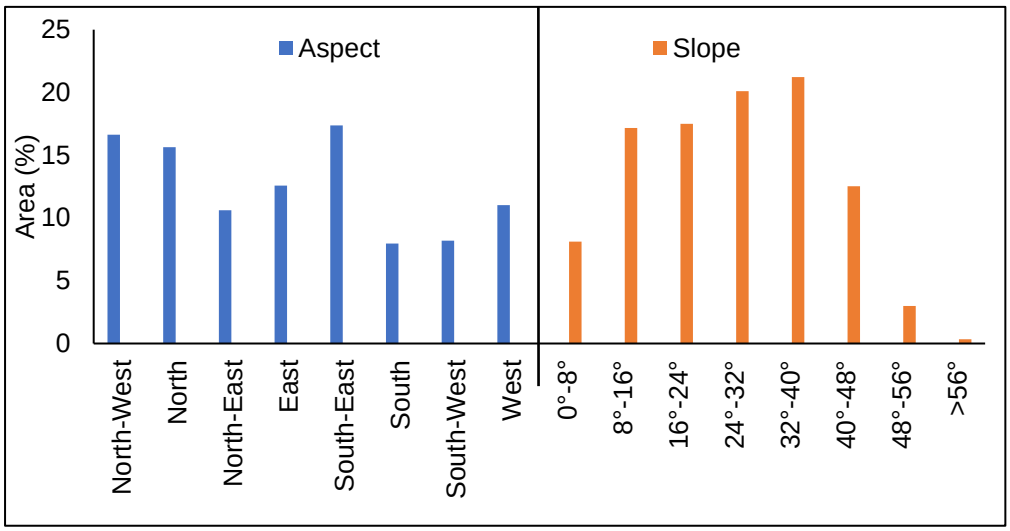

749

750 **Figure 3:** The basin's area (%) vs aspect and slope distribution (Kumar et al., 2018).

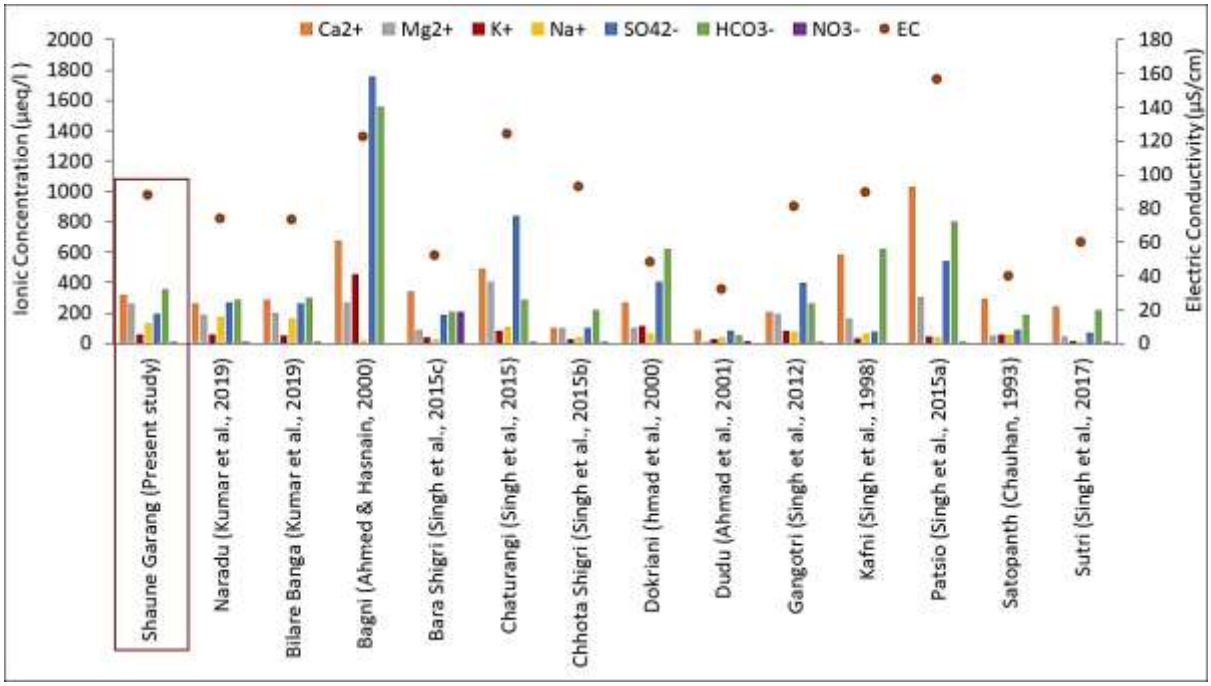

751

752 **Figure 4:** The average hydro-geochemical characteristics of glacial meltwater from Shaune
753 Garang Glacier and its comparison with the other Himalayan glaciers.

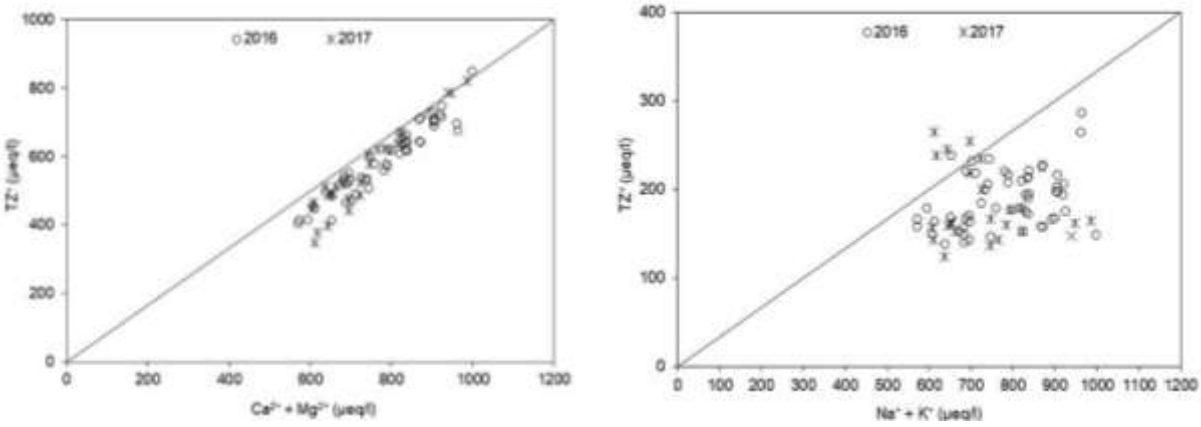

754

755 **Figure 5:** Scatter plot of (Ca^{2+}+Mg^{2+}) against TZ^{+} and (Na^{+}+K^{+}) against total cation (TZ^{+})
756 during the study period of 2016 and 2017 from Shaune Garang glacier catchment.

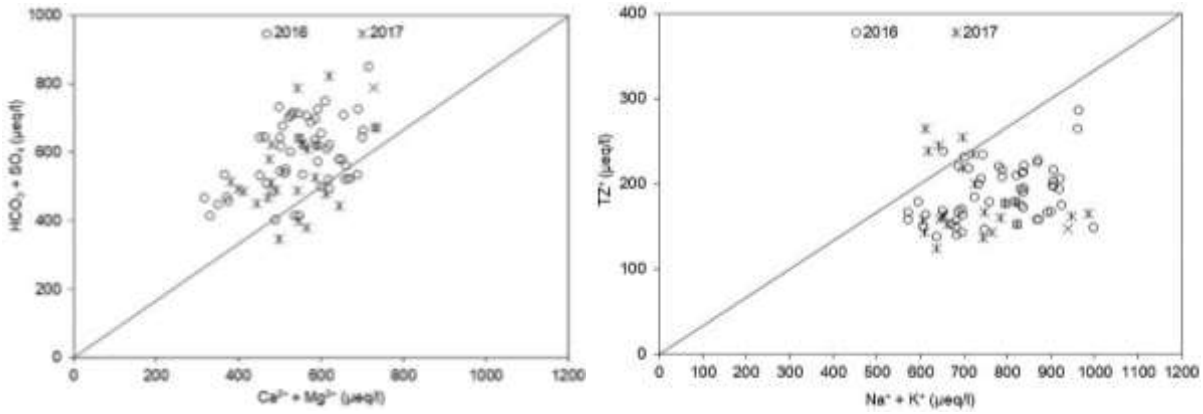

Figure 6: Scatter plot of (Ca^{2+}+Mg^{2+}) against (HCO_3^-+SO_4^{2-}) and (Ca^{2+}+Mg^{2+}) against SO_4^{2-} during the study period of 2016 and 2017 from Shaune Garang glacier catchment.

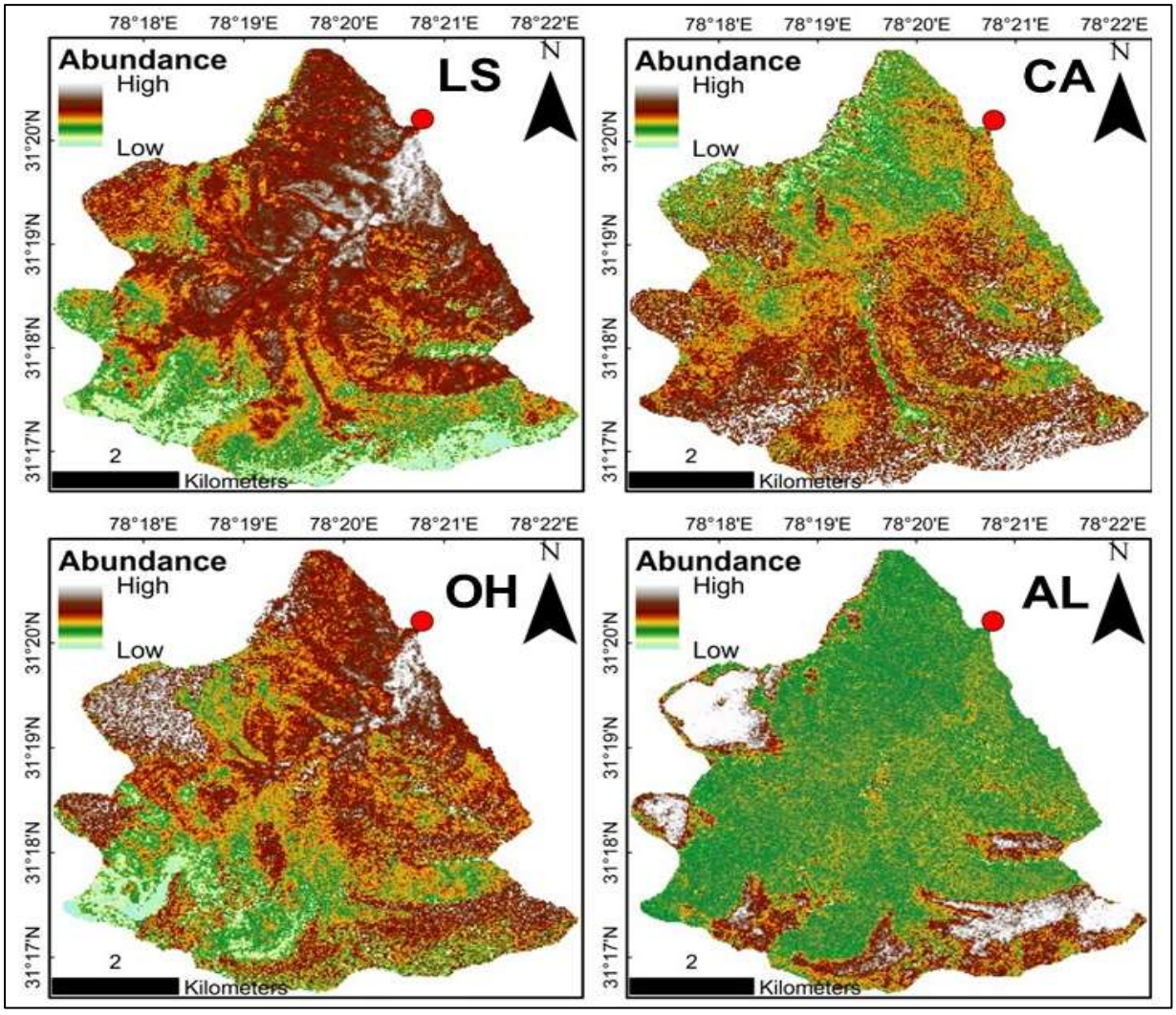

Figure 7: Mineralogical maps based on the radiance properties of ASTER SWIR of Shaune Garang catchment. The indexes are represented through LS, CA, AL, and OH for layered silicate, calcite, Alunite, and hydroxyl bearing materials.

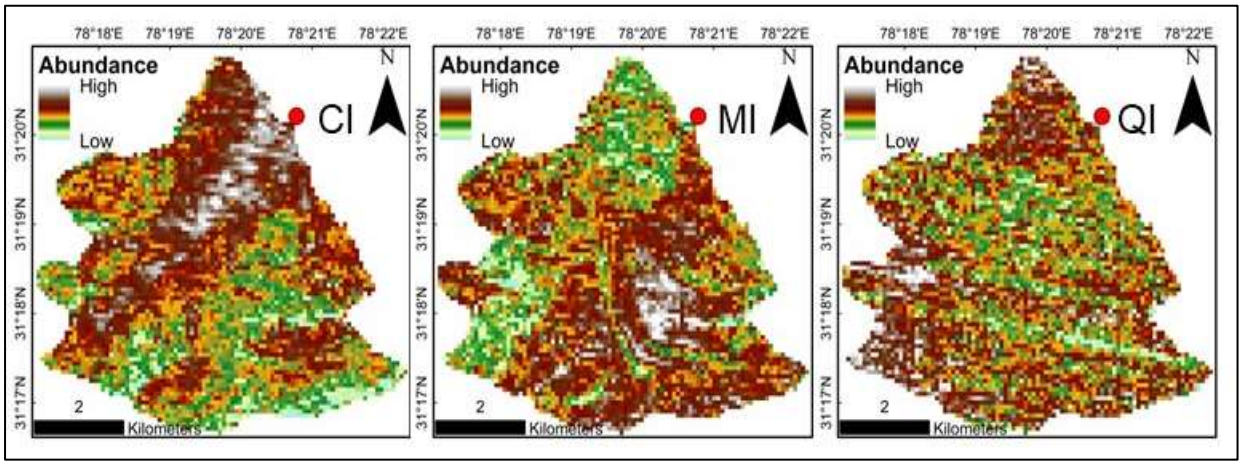

Figure 8: Mineralogy maps based on the "ASTER TIR" of Shaune Garang catchment's radiance properties. The indexes are "Carbonate Index (CI), Quartz Index (QI), and Mafic Index (MI)".

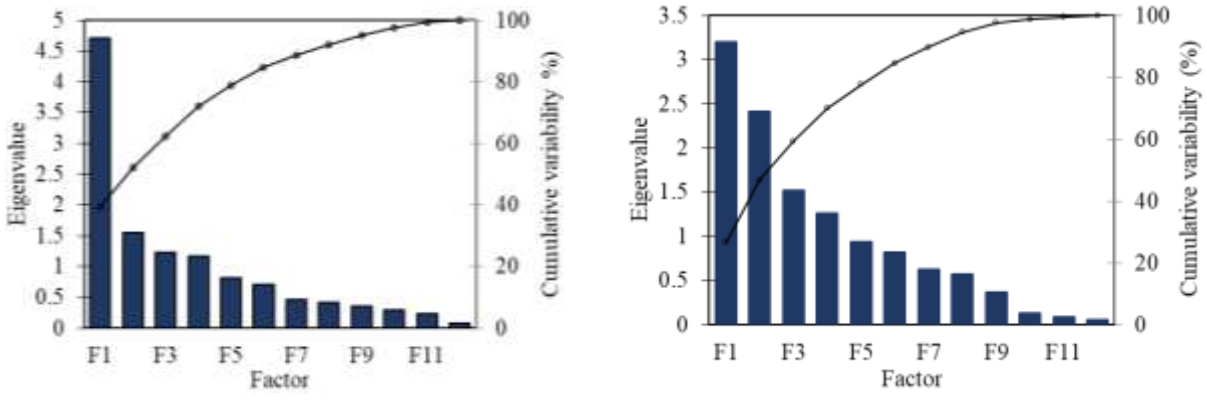

Figure 9: Scree plot graph between eigenvalue and factors for 2016 and 2017.

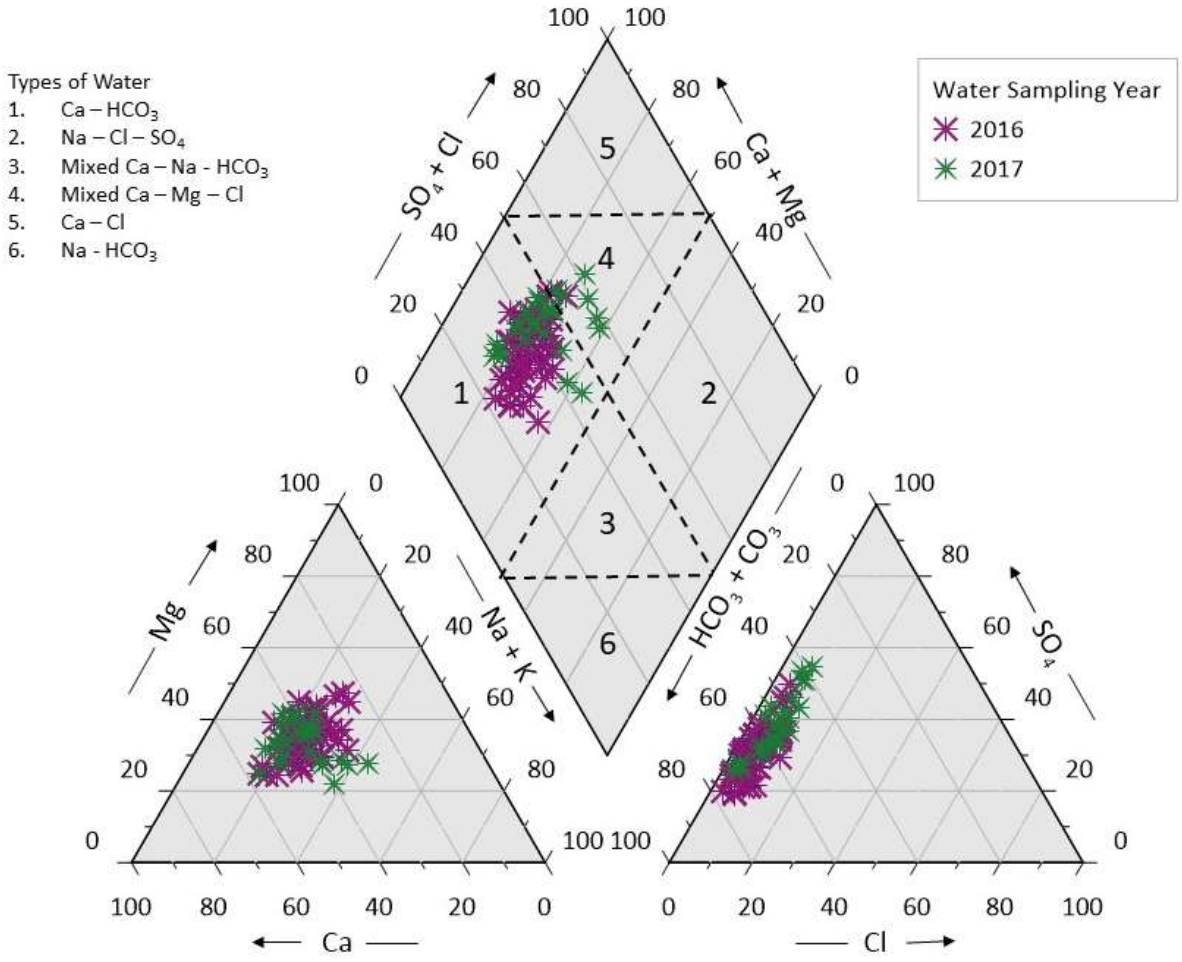

Figure 10: Piper plot for concentration of ions during study period 2016 and 2017 in the Shaune Garang catchment.

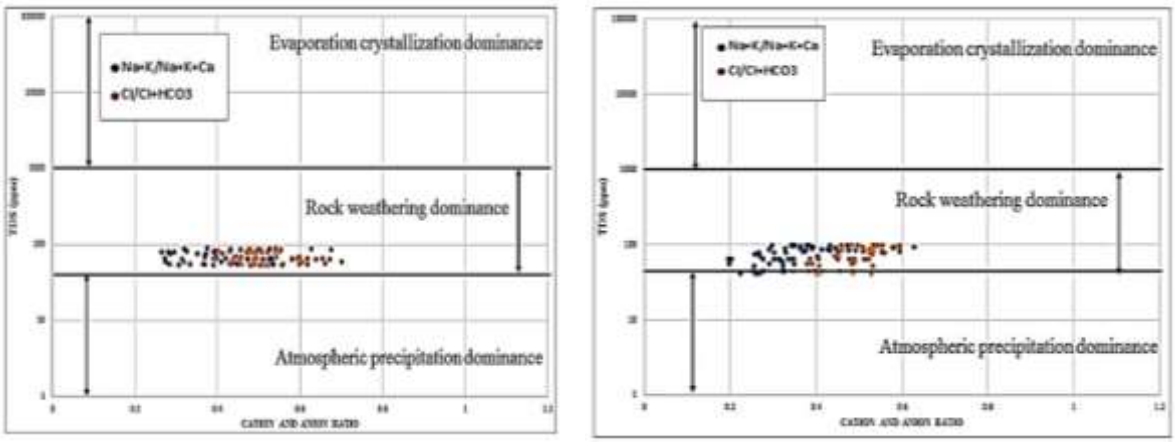

Figure 11: Gibb's diagram represents controlling factors of meltwater quality.